JACS
JOURNAL OF THE AMERICAN CHEMICAL SOCIETY

ARTICLE

pubs.acs.org/JACS

Electrochemistry, Electrogenerated Chemiluminescence, and Excimer Formation Dynamics of Intramolecular π-Stacked 9-Naphthylanthracene Derivatives and Organic Nanoparticles

Jungdon Suk,[†] Zhiyong Wu,[‡] Lei Wang,[*,‡] and Allen J. Bard[*,†]

[†]Center for Electrochemistry and Department of Chemistry and Biochemistry, The University of Texas at Austin, Austin, Texas 78712, United States

[‡]Wuhan National Laboratory for Optoelectronics, Huazhong University of Science and Technology, Wuhan, P.R. China

Supporting Information

ABSTRACT: We report the electrochemical characterization and the observation of excimer emission from a series of 9-naphthylanthracene-based dimer- and trimer-bridged high steric hindrance aromatic groups during photoluminescence (PL) measurements in the solid state and in solution electrogenerated chemiluminescence (ECL) measurements. Cyclic voltammetry of 4,4′-bis(9-(1-naphthyl)anthracen-10-yl)biphenyl (**4A**) and 1,3,5-tris(9-(1-naphthyl)anthracen-10-yl)benzene (**4C**) showed two or three reversible, closely spaced one-electron transfers on oxidation in dichloromethane. The ECL emission spectra of **4A** and **4C** resulting from the annihilation reaction in benzonitrile showed two bands: one at the same wavelength as the PL peak in the solution state, and a broad band at longer wavelength. With a coreactant, such as peroxydisulfate, ECL spectra showed a single peak that was less broad in shape. PL measurement in the solid state and measurement of representative time traces of PL intensity, lifetimes, and picosecond time-correlated single-photon counting confirmed excimer emission at long wavelength. A reprecipitation method was used to prepare well-dispersed organic nanoparticles (NPs) of **4A** in both aqueous and acetonitrile solutions. The smallest stable size of NPs produced was ~15 ± 6 nm, as analyzed by transmission electron microscopy. These organic NPs produced stable and weak ECL emission from the annihilation reaction in both aqueous and MeCN solutions. With a coreactant, such as peroxydisulfate, the ECL signal on reduction was sufficiently strong to obtain an ECL spectrum.

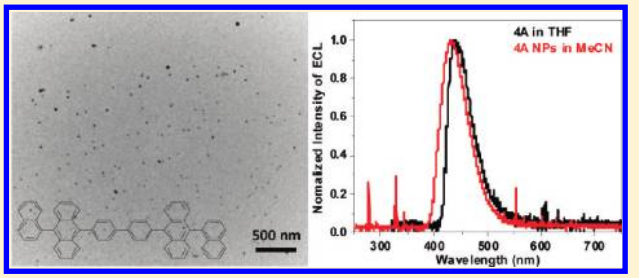

INTRODUCTION

Aromatic hydrocarbons have been widely used in electrogenerated chemiluminescence (ECL) and solid-state electroluminescence (EL) studies. Since the first report of EL, by Pope et al. in 1963,[1] anthracene, a fluorescent material emitting at about 400 nm, has been used as a precursor to synthesize blue-emitting materials with high device stability and high EL efficiency.[2] There have been several previous reports of new anthracene derivatives that have been developed and investigated to tune their photophysical properties, such as color purity, high efficiency, and good stability. Among these, the series of 9-naphthylanthracene-based dimer and trimer compounds show interesting and potentially useful EL properties.[3] Some anthracene derivatives, such as 9,10-diphenylanthracene (DPA) and naphthacene, which have bulky functional groups, show little photoluminescence (PL) excimer formation due to steric hindrance. However, a secondary broad peak at longer wavelengths in ECL studies, which is not seen in PL of solution, can be observed in sterically hindered compounds in some cases. Moreover, due to their high PL quantum yields, these compounds are good candidates for use as blue-light emitters in ECL devices, if they show stable radical cations and anions in solution.

ECL involves the generation of products, such as electrogenerated radical ions, at an electrode surface that undergo an electron-transfer reaction and emit light.[4] This process has been extensively investigated in studying radical ion formation and stability and intermolecular electron transfer. If the radical ion annihilation energy is enough to populate an excited singlet state, this mechanism is called the S-route, or an "energy-sufficient system". This type of ECL reaction, where the potential is swept or stepped in both the reducing and oxidizing directions, has been studied for many systems, and these mechanisms are well understood. If the energy is not sufficient to populate the excited singlet state but can generate the triplet state, emission can result from the triplet−triplet annihilation. This is called the T-route, or an "energy-deficient system". Scheme 1 shows the S-route and T-route mechanisms.

Another ECL emission mechanism is called the E-route because it results in excimer or exciplex emission.[4] An excited-state dimer or "excimer" is formed in PL by the association of an excited fluorophore with another fluorophore in its ground state.[5] In the case of most aromatic molecules, excimer emission

Received: April 22, 2011
Published: August 01, 2011

Scheme 1

S-route

$$A - e^- \rightarrow A^{\bullet +} \quad \text{(formation of radical anion)} \quad (1)$$

$$A + e^- \rightarrow A^{\bullet -} \quad \text{(formation of radical cation)} \quad (2)$$

$$A^{\bullet +} + A^{\bullet -} \rightarrow {}^1A^* + A \quad \text{(singlet excited state formation)} \quad (3)$$

$${}^1A^* \rightarrow A + h\nu \quad \text{(ECL emission from singlet state)} \quad (4)$$

T-route

$$A^{\bullet +} + A^{\bullet -} \rightarrow {}^3A^* + A \quad \text{(triplet excited state formation)} \quad (5)$$

$${}^3A^* + {}^3A^* \rightarrow {}^1A^* + A \quad \text{(triplet} - \text{triplet annihilation)} \quad (6)$$

Scheme 2

E-route

$$A^{\bullet +} + A^{\bullet -} \rightarrow (A_2^*) \quad \text{(excimer formation)} \quad (7)$$

$$(A_2^*) \rightarrow 2A + h\nu \quad \text{(excimer emission)} \quad (8)$$

typically produces a broad fluorescence band at longer wavelengths, the broadness resulting from the absence of a stable dimeric ground state.[6] In PL, excimers are produced by relatively long-lived monomer excited states and are favored by high ground-state concentrations.[7] Many polyaromatic hydrocarbons, such as anthracene,[8] pyrene,[9] and perylene,[10] also produce excimer emission in the ECL spectrum by the E-route mechanism.[4] The formation of excimers in ECL by ion annihilation can be a very efficient process when two aromatic systems are brought into proximity.[11] The E-route mechanism was proposed to explain ECL emission with broad features and red-shifted emission with longer lifetimes.[12,13] Long-wavelength ECL, which cannot be seen in PL, generally results either from side products of the electrochemical reaction or from the formation of excimer. For example, long-wavelength ECL of anthracene was attributed to energy transfer to a radical cation decomposition product.[14] Scheme 2 shows the E-mechanism.

Most ECL studies of aromatic hydrocarbons are carried out in nonaqueous solvents like acetonitrile (MeCN) under conditions of very low water and oxygen concentrations.[4] These cannot be carried out in aqueous media because of the low solubility of aromatic compounds in water and the high reactivity of their radical ions with water and oxygen. The preparation of organic nanoparticles (NPs) dispersed in water raises the possibility of studying their behavior and producing ECL. ECL from NPs of the aromatic hydrocarbons rubrene and DPA in an aqueous solution has been reported.[15]

In this paper, we report electrochemical, photophysical, and ECL properties of two new compounds based on aromatic bridged anthracene derivatives. We also probe excimer formation dynamics by measuring the ECL in solution by both ion annihilation and coreactant processes, the fluorescence lifetimes, and fluorescence intensity trajectories in thin solid films. We also find that **4A** can form stable organic NPs in both water and MeCN by a reprecipitation method, and we have studied the spectroscopic, electrochemical, and ECL characteristics of **4A** NPs.

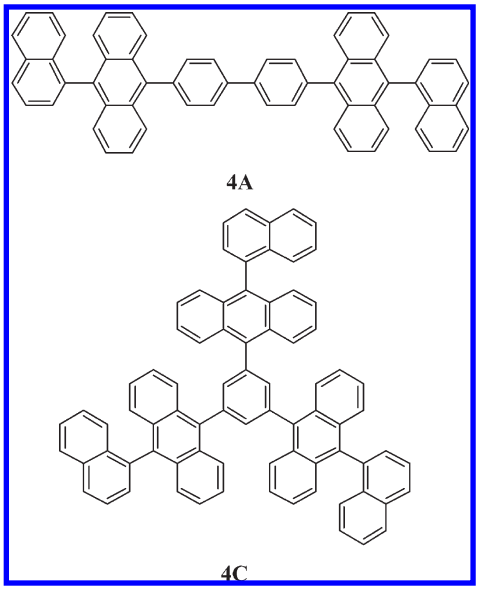

Figure 1. Molecular structures of compounds **4A** and **4C**.

EXPERIMENTAL SECTION

Chemicals. The synthesis of **4A** and **4C**, whose structures are shown in Figure 1, has been described previously.[3] Anhydrous benzonitrile (BZN, 99%) and dichloromethane (DCM, 99.93%) were obtained from Aldrich (St. Louis, MO). Tetrahydrofuran (THF) was distilled from sodium/benzophenone and degassed by two freeze−pump−thaw cycles. Tetra-*n*-butylammonium hexafluorophosphate ($TBAPF_6$) was obtained from Fluka and used as received. All solutions were prepared in a He atmosphere glovebox (Vacuum Atmospheres Corp., Hawthorne, CA) and placed in an airtight cell for measurements completed outside of the box. The film samples for spectroscopic measurements were fabricated by vacuum deposition of the material at 10^{-6} Torr onto thoroughly cleaned glass coverslips.

Characterization. Electrochemical methods such as cyclic voltammetry (CV) and multipotential step were performed with a three-electrode cell linked to a CH Instruments model 660 electrochemical workstation (Austin, TX). The electrochemical cell consisted of a Pt wire counter electrode, an Ag wire quasi-reference electrode (QRE), and a 2 mm diameter Pt disk (surface area = 0.024 cm^2) inlaid in a glass working electrode (WE). The Pt WE was bent at a 90° angle (J-type electrode) so that the electrode surface faced the detector in the ECL experiments. Before each experiment, the WE was polished on a felt pad with 1, 0.3, and 0.05 μm alumina (Buehler, Ltd., Lake Bluff, IL), sonicated in deionized water and ethanol for 1 min each, dried in an oven at 100 °C, and then transferred into the glovebox. All potentials were calibrated against a saturated calomel electrode (SCE) by the addition of ferrocene as an internal standard at the end of all measurements, taking E°_{Fc/Fc^+} = 0.342 V vs SCE.[16] For chronoamperometry experiments, a 25 μm diameter Pt ultramicroelectrode (UME) was used as a WE. Digital simulations of cyclic voltammograms were performed using DigiSim 3.03 (Bioanalytical Systems, Inc., West Lafayette, IN).

Steady-state absorption spectra were taken using a UV−vis−NIR spectrometer (Cary model 5000, Varian), and fluorescence spectra were obtained using a Perkin-Elmer LS55 luminescence spectrometer with an excitation wavelength of 375 nm. The relative fluorescence efficiencies were determined with respect to DPA as a standard (λ_{exc} = 380 nm, Φ_{PL} = 0.91 in benzene).[17] A picosecond time-correlated single-photon counting (TCSPC) system was used for time-resolved fluorescence decay measurements in which a tunable Ti:sapphire laser (tuned to 740 nm, 100 fs pulse width, 80 MHz repetition rate; Spectral Physics, Mai Tai, Newport Corp., Irvine, CA) was frequency-doubled with a BBO (β-barium borate) crystal (0.5 mm, Castech Inc., China) and then used to excite the sample. Fluorescence lifetime was determined using a commercial confocal laser scanning microscope (Olympus FV1000) equipped with an aprochromatic objective (Olympus 60×, oil immersion, numerical aperture = 1.42) and a 16-channel multispectral detection assembly (PML-SPEC, Becker & Hickl, Germany) connected to a TCSPC module (SPC 830, Becker & Hickl). The SPCM software (Becker & Hickl) was used to allow fluorescence lifetime imaging during the scanning process. Lifetime decay curves were analyzed with SPC Image (Becker & Hickl) or other software. The full width at half-maximum (fwhm) of the instrument response function was typically 150 ps in our TCSPC system.

ECL transients were simultaneously recorded by an Autolab electrochemical workstation (Eco Chemie, The Netherlands) coupled with a photomultiplier tube (PMT, Hamamatsu R4220p, Japan). The PMT was supplied with −750 V with a high-voltage power supply series 225 (Bertan High Voltage Corp., Hucksville, NY). ECL transients were generated by pulsing the electrode 80 mV beyond the diffusion-limited peak potentials for oxidation and reduction peaks or by pulsing the potentials with the same current. For obtaining the ECL spectra, the detector was a charge-coupled device camera (Princeton Instruments, SPEC-32). The integration time for all spectra was 5 min, and the slit width was 0.75 μm. The camera was cooled with liquid nitrogen between −100 and −120 °C, and the spectral wavelengths were calibrated using a mercury lamp (Oriel, Stratford, CT).

Synthesis of 4A NPs. The reprecipitation method was used for NP synthesis.[18] **4A** NPs were synthesized by injecting 800 μL of **4A** in THF (5×10^{-5} M) solution with a 50 μL microsyringe (Hamilton Co., Reno, NV) into 10 mL of warm, deionized water (60−70 °C) or anhydrous MeCN under vigorous stirring. The dispersion of NPs in MeCN was prepared in a He atmosphere glovebox (Vacuum Atmospheres Corp.) and placed in an airtight cell with a Teflon cap for measurements completed outside the box. The resulting NP solution was filtered through a 0.22 μm pore membrane filter (Millex GP, PES membrane).

Size Measurement. Transmission electron microscopy (TEM) was performed with a Tecnai Spirit BioTwin microscope (FEI Co., The Netherlands) at an accelerating voltage of 80 kV. TEM samples were prepared by dropping 5 μL of fresh NP solution onto a 400 mesh carbon-coated copper TEM grid. Dynamic light scattering experiments with the particles were attempted but did not give consistent results.

Table 1. Electrochemical Data

	$E_{1/2}$ (V vs SCE)						
	$A/A^{\bullet-}$	$A/A^{\bullet+}$	D (cm^2/s)	n	E_g[a] (eV)	E_{HOMO}[b] (eV)	E_{LUMO}[c] (eV)
4A	−2.14	1.24	6×10^{-6}	2	−3.38	−6.0	−2.62
4C	−1.98	1.25	4×10^{-6}	3	−3.23	−6.01	−2.78

[a] From CV. [b] The HOMO values are calculated on the basis of the value of −4.8 eV in a vacuum for ferrocene. [c] From the reduction wave.

RESULTS AND DISCUSSION

Electrochemistry. Electrochemical results are summarized in Table 1. CV was used to determine the stability of the radical ions in the solution and to find the energy of annihilation in ECL. The electrochemistry of the two compounds **4A** and **4C** was studied in various solvents such as BZN, DCM, and THF. These compounds had poor solubilities in both pure MeCN and MeCN−benzene mixtures, which are favored solvents in ECL studies because of their wide electrochemical window. Although these compounds have good solubility in DCM and THF, these solvents have smaller potential windows for the generation of very reducing or oxidizing species and the observation of radical ion annihilation.[19] BZN, like MeCN, is a good solvent in which to observe electrochemically generated radical cations and anions; however, it has a smaller cathodic potential window for reductions than MeCN. Compound **4A** dissolved only in a hot (>90 °C) solution of BZN, but compound **4C** dissolved at room temperature in BZN. Figure 2 shows the CVs of the two compounds with 0.1 M $TBAPF_6$ in anhydrous BZN (background CV is shown in Supporting Information, Figure S1) The CVs of **4A** and **4C** at a scan rate, ν, of 0.5 V/s showed a quasi-reversible oxidation wave and an irreversible reduction wave with very similar half-wave potentials. With higher ν, e.g., >1 V/s, the oxidation wave became reversible. The quasi-reversibility and irreversibility of CV waves in BZN indicate the instability of radicals or interference of the solvent by limiting the potential range or perhaps reacting with trace impurities.

When DCM was used to study the oxidation and THF was used for the reduction, the CVs of 0.5 mM **4A** and **4C** produced reversible waves (Figures 3 and 4). Upon scanning to positive potentials in DCM, the oxidation of **4A** showed a nernstian wave that could be simulated (Supporting Information Figure S3) as

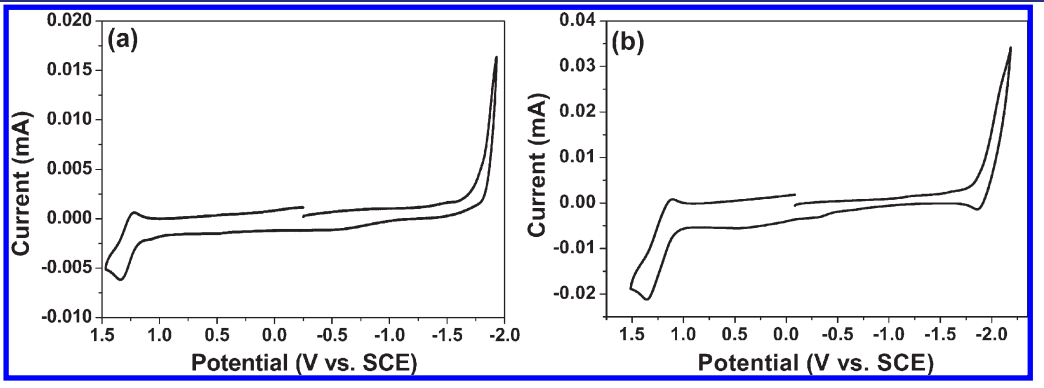

Figure 2. Cyclic voltammograms (a) of 0.5 mM **4A** in hot BZN and (b) of 0.5 mM **4C** in room-temperature BZN with 0.1 M $TBAPF_6$. WE, Pt disk; CE, Pt coil; RE, Ag wire as a QRE; scan rate, 0.5 V/s.

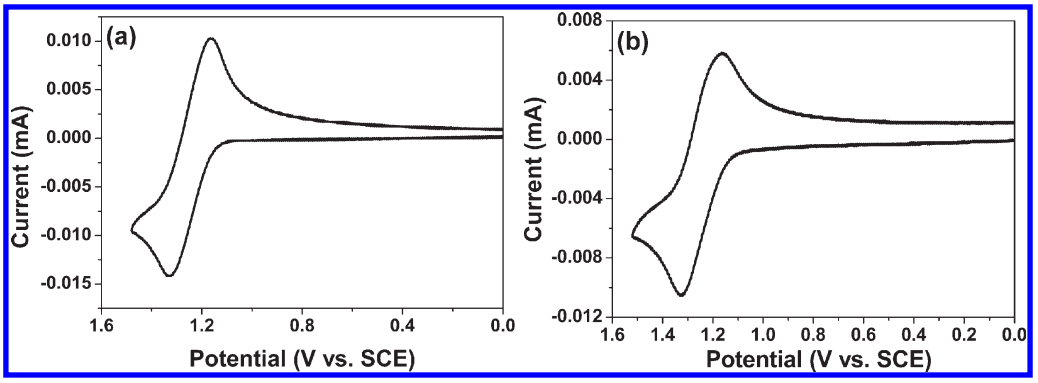

Figure 3. Cyclic voltammograms for oxidation of (a) 0.5 mM **4A** and (b) 0.4 mM **4C** in DCM with 0.1 M $TBAPF_6$. WE, Pt disk; CE, Pt coil; RE, Ag wire as a QRE; scan rate, 0.5 V/s.

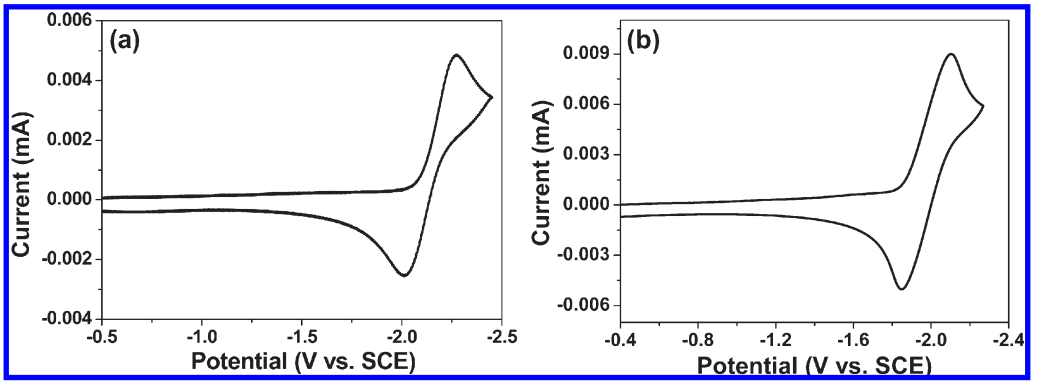

Figure 4. Cyclic voltammogram for reduction of (a) 0.5 mM **4A** and (b) 0.5 mM **4C** in THF with 0.1 M $TBAPF_6$. WE, Pt disk; CE, Pt coil; RE, Ag wire as a QRE; scan rate, 0.5 V/s.

two sequential one-electron transfers at 1.24 V vs SCE. The oxidation of **4C** showed very similar behavior at 1.25 V, probably involving the same 1-naphthyl moiety. The observed peak separation for the oxidation peaks was ~160 mV, larger than the expected value for nernstian behavior for one-electron-transfer reversible peak separation, 59 mV.[20] This larger peak separation can be attributed to uncompensated resistance (R_u = 3240 Ω), but also to the multi-electron-transfer system. The multi-electron transfer was confirmed by chronoamperometric experiments with a UME (Supporting Information Figure S2) and digital simulation (Supporting Information Figures S3−S6), as discussed below. The peak current ratio (i_{pa}/i_{pc}) of the oxidation waves of the two compounds was approximately unity with a 500 mV/s scan rate, indicating the absence of subsequent chemical reactions and good stability of the radical ions. Moreover, scan rate studies (Supporting Information Figure S7) showed that the peak currents of the oxidation wave were proportional to the square root of the scan rate ($v^{1/2}$). Unlike the irreversible reduction wave seen in BZN, a negative scan in THF showed a reversible reduction wave at $E_{1/2}$ = −2.14 V for **4A** and −1.98 V for **4C** vs SCE.

The number of electrons, n, in the oxidation wave was determined by comparing the transient current, $i_d(t)$, and the steady-state current, $i_{d,ss}$, in a chronoamperometric experiment with **4A** at a UME (Supporting Information Figure S2).[21] Figure S2 shows the linear scan voltammetry (a) and the experimental ratio $i_d(t)/i_{d,ss}$ vs $t^{-1/2}$ (b) for the oxidation with 0.5 mM **4A** on a 25 μm radius Pt UME in DCM/0.1 M $TBAPF_6$. The CV at a Pt UME shows a nernstian reaction shape with a clear steady-state current for the oxidation. With this technique, n can be determined without knowledge of the bulk concentration and the diffusion coefficient, D. The results from this technique for the oxidation of **4A** and **4C** yield n = 2.04 and 3.29, consistent with overall two- and three-electron oxidations and diffusion coefficients of 6×10^{-6} and 4×10^{-6} cm^2/s, respectively.

Figures S3−S6 in the Supporting Information compare experimental and simulated oxidation and reduction CVs of **4A** and **4C** at different scan rates from 50 mV/s to 10 V/s. Digital simulation of CVs with different scan rates helped to obtain information about the potentials of the reaction steps. The uncompensated resistance and capacitance were found by a potential step where no faradaic reactions occurred (0.4 V vs SCE) and the simulation was corrected for resistance (3240 Ω) and capacitance (500 nF). The fit between experimental and simulated data for sequential electron-transfer mechanisms was good: for **4A**, $E^\circ_{1,ox}$ = 1.22 V, $E^\circ_{2,ox}$ = 1.25 V vs SCE; for **4C**, $E^\circ_{1,ox}$ = 1.17 V, $E^\circ_{2,ox}$ = 1.21 V (Supporting Information Figure S3), and $E^\circ_{3,ox}$ = 1.25 V vs SCE. (Supporting Information Figure S4). The reduction of **4A** in THF showed a nernstian wave at all scan rates and also a sequential two-electron-transfer mechanism, consistent with potentials of $E^\circ_{1,red}$ = −2.08 V and $E^\circ_{2,red}$ = −2.13 V vs SCE (Supporting Information Figure S5). The reduction of **4C** in THF (Supporting Information Figure S6) occurs by a sequential, three-electron transfer with $E^\circ_{1,red}$ = −1.97 V, $E^\circ_{2,red}$ = −2.02 V, and $E^\circ_{3,red}$ = −2.07 V vs SCE. In the simulation, all the electron-transfer reactions were considered fast ($k^\circ \geq 10^4$ s^{-1}), and α values were taken to be 0.5. The results, i.e., the single oxidation and

reduction wave with splittings ~160 mV, showed little delocalization among the 9-naphthylanthracene groups via the biphenyl (**4A**) or the benzene (**4C**) group because the groups are twisted out of the plane due to strong steric hindrance. This is consistent with the topology seen for **4A** and **4C** in the crystal structure.[3]

Spectroscopy. The normalized UV−vis absorption and fluorescence (PL) spectra for **4A** and **4C** are shown in Figure 5. The absorption and PL spectra of compounds were measured in BZN, the same solvent as that used for the electrochemical measurements. The optical properties, absorption and emission maxima, extinction coefficients, fluorescence quantum yields, and optical energy gap are recorded in Table 2. The three strong vibronic structure peaks between 300 and 400 nm are assigned to the bands characteristic of anthracene and its derivatives, i.e., the S0→S1 transition of the anthracene moiety.[22] The absorbance of two compounds showed three peaks around 357, 377, and 400 nm. The fluorescence of these compounds, taken with excitation at the absorption maxima around 400 nm, did not display the mirror image of the absorbance spectra. The PL spectra of **4A** featured an intense and broad blue emission peak with λ_{max} = 423 nm. The PL spectra of **4C** featured two intense peaks with λ_{max} = 416 and 436 nm. **4C** showed a 2 nm blue shift as compared to **4A**, probably because the propeller twist structure of the trimer contributes to distortion of the π-conjugated system. No other luminescence above 500 nm was found in solution. However, the solid-state emission bands of these compounds showed very broad maxima around 450 nm and an additional broad peak between 500 and 570 nm with a long tail until 650 nm.[3]

The PL of **4A** in the powder or film state showed a new peak at longer wavelengths, whose intensity showed strong thickness-dependent effects. The intensity of the emission band at longer wavelengths increased substantially with a thicker film. As shown in Supporting Information Figure S8a, the intensity of the new peak (535 nm) for **4A** increased 3-fold when the film thickness increased from 25 to 100 nm. In the powder state, the component of the new peak (535 nm) of the PL had almost the same intensity as the main peak of the monomer. Meanwhile, a shoulder at 570 nm became much clearer. This can be ascribed to a surface/volume ratio decrease in the **4A** film as the film thickness increases on the nanoscale from 25 to 100 nm. The surface is known to quench excited states through dissociation and nonradiative thermal emission processes. Because of weak coulomb binding energies and also strong electron−phonon coupling, the excimers are more sensitive to surface quenching as compared to excitons. As a result, increasing the film thickness or decreasing the surface/volume ratio can lead to an enhancement in the light emission from excimers. However, in the case of **4C**, the new additional peak at long wavelength was very weak and its intensity changed little when the film thickness increased from 25 to 100 nm (Figure S8b). Because of the propeller topology of **4C**, the formation of excimer is difficult, so it induces weak intensity at the secondary peak, and the intensity changes had little dependence on the film thickness.

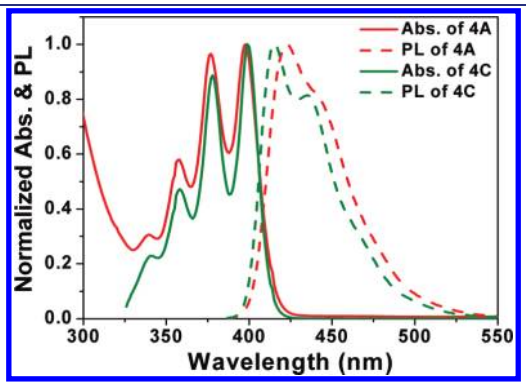

Figure 5. Absorbance (solid line) and fluorescence spectra (dashed line) of (a) **4A** (red) and (b) **4C** (green) in BZN. Emission spectra were excited at the absorption maxima.

To probe the excimer formation dynamics of aromatic bridged anthracene derivatives more deeply,[23] we measured the fluorescence lifetimes of **4A** and **4C** in the solid thin films (thickness 40 nm) using the TCSPC technique (scan range 400−600 nm) with an excitation wavelength of 370 nm. Representative time traces of the fluorescence intensities and lifetimes of the compound **4A** and **4C** are shown in Figures 6 and 7. The fluorescence lifetime in the trace was obtained by fitting fluorescence decay profiles that were constructed from fluorescence photons per each integration time of 1 s. From the single-pixel fluorescence lifetime decay profiles of **4A** (Figure 6a) and **4C** (Figure 7a), we found biexponential fluorescence decay components [e.g., τ_1 = 0.19 ns, amplitude = 98.1%, τ_2 = 2.32 ns, amplitude = 1.9% for **4A** (Figure 6b) and τ_1 = 0.18 ns, amplitude = 95.9%, τ_2 = 0.9 ns, amplitude = 4.1% for **4C** (Figure 7b)], which were associated with monomer and excimer states. However, the amplitude of components obtained from biexponential fitting cannot represent the real amplitude because of the influence of the complicated single-pixel microenvironment. Therefore, all the fitted lifetimes in 256 pixels of **4A** and **4C** were assembled into a frequency histogram. For **4A**, the complete lifetime distribution can be categorized into two Gaussian distributions with mean lifetimes of 0.25 and 0.83 ns, respectively. The first distribution of lifetimes for the typical monomer covered the largest area (68%) of the whole histogram from the typical fluorescence upon photoexcitation of **4A**. Furthermore, the second distribution (32%), ranging from 0.5 to 1.4 ns, indicated excimers induced by interaction between the excited and ground states. Under the same experimental conditions, the fluorescence lifetime distribution of **4C** consisted of two sections: monomer emission and weakly coupled excimer emission. The monomer emission, with a mean lifetime of 0.23 ns, covered the largest area (76.8%), and the weakly coupled excimer emission (23.2%) was distributed throughout the whole histogram. The detailed fractions of monomer and excimer for **4A** and **4C** are listed in Table 3, and fluorescence decay times and relative amplitudes of both compounds are listed in Table 4. Compared to **4A**, the broad lifetime histogram of **4C** ranged from about 0.18 to 0.32 ns, which is narrower than for **4A**.

Table 2. Spectroscopic and ECL Data

	$\lambda_{max(abs)}$ (nm)	$\lambda_{max(PL)}$ (nm)	Φ_{PL} [a]	$\lambda_{max(ECL)}$ (nm)	$\Phi_{r,ECL}$ [b]	$-\Delta G_{ann}$ [c] (eV)	$-\Delta H_{ann}$ [d] (eV)	E_s [e] (eV)
4A	357, 377, 400	423	0.64	477	0.0044	3.38	3.28	2.93
4C	357, 377, 400	416, 436	0.68	479	0.0045	3.23	3.18	2.98

[a] Φ_{PL} is the relative PL compared to DPA. $\Phi_{PL,DPA}$ = 0.91 in benzene. [b] $\Phi_{r,ECL}$ is the relative ECL compared to DPA. $\Phi_{ECL,DPA}$ = 0.014. [c] $-\Delta G_{ann} = E_{pa}^{ox} - E_{pc}^{red}$. [d] $-\Delta H_{ann} = -\Delta G_{ann} - 0.1$. [e] $E_S = 1239.85/\lambda_{max}^{PL}$ (nm).

dx.doi.org/10.1021/ja203731n |J. Am. Chem. Soc. 2011, 133, 14675–14685

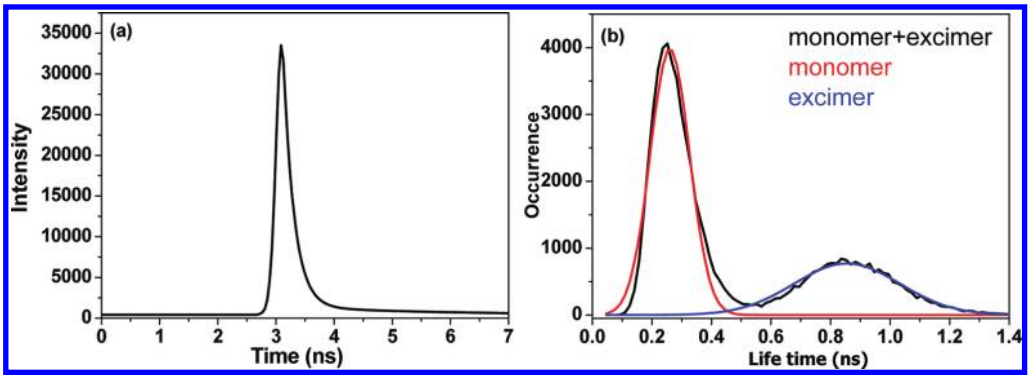

Figure 6. Fluorescence behavior of **4A** in solid film (40 nm). (a) Fluorescence intensity trajectories of **4A**, with their corresponding lifetime decay profiles in single pixels. (b) Fluorescence lifetime distribution. The fluorescence lifetimes in the distribution were obtained by fitting all photons for every 1 s in 256 pixels.

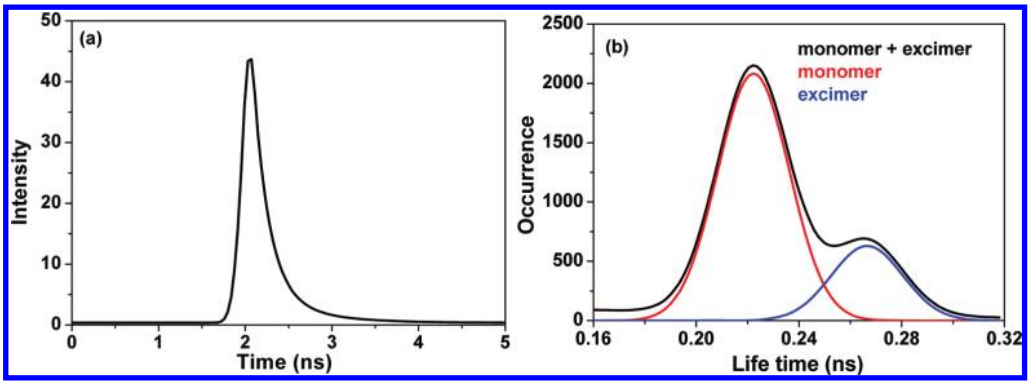

Figure 7. Fluorescence behavior of **4C** in solid film (40 nm). (a) Fluorescence intensity trajectories of **4C**, with their corresponding lifetime decay profiles in single pixels. (b) Fluorescence lifetime distribution. The fluorescence lifetimes in the distribution were obtained by fitting all photons for every 1 s in 256 pixels.

Table 3. Fluorescence Lifetime Distribution of 4A and 4C and Their Component Fractions

	peak no.[a]	τ (ns)	fwhm (ns)	fraction (%)
4A	1	0.25	0.16	68
	2	0.83	0.42	32
4C	1	0.23	0.034	76.8
	2	0.26	0.032	23.2

[a] Peaks 1 and 2 are associated with the monomer and excimer states, respectively.

Table 4. Fluorescence Decay Times (ns)[a] and Relative Amplitude (%) of 4A and 4C

	4A	4C
τ_1	0.185 ns, 98.1%	0.18 ns, 95.9%
τ_2	2.32 ns, 1.9%	0.903 ns, 4.1%

[a] τ_1 and τ_2 are associated with the monomer and excimer states, respectively.

The main peak of excimer lifetime is at 0.26 ns, indicating that the excimer state of **4C** becomes more unstable and energetically higher than that of **4A**, and as a consequence, the fluorescence lifetime becomes shorter. These results are also a consequence of the propeller topology of **4C**, which makes the molecular excited state more energetic. A highlight of the bulk lifetime distribution measurements is the appearance of longer lifetime components in the solid state, showing that the formation of excimer depends on various torsional angles and microenvironments.

Electrogenerated Chemiluminescence (ECL). *Ion Annihilation.* Figure 8 shows the ECL spectra (pink line) of **4A** and **4C** in BZN with 0.1 M $TBAPF_6$ as supporting electrolyte during repeated pulsing (pulse width = 0.1 s) between potentials where the oxidized and reduced forms were alternately produced (with a 5 min integration time). The ECL spectra of **4A** and **4C** from the annihilation reaction showed two bands. The maxima of the shorter wavelength peak in all ECL spectra were close to the PL spectra (blue line) of the solution; the 30 nm difference between the PL and ECL is probably caused by an inner-filter effect from the different solution concentrations used in the PL and ECL measurements and by the difference in resolution between the two instruments where the spectra were collected.[24] The broad secondary band of ECL from **4A** and **4C** at much longer wavelengths did not appear in the PL, which did not show emission beyond 500 nm. The maxima of the first ECL peaks were at 452 nm for **4A** and 446 nm for **4C**. Moreover, the long-wavelength emissions were quite broad and centered at 585 nm for **4A** and 564 nm for **4C**. The long-wavelength ECL emission of these two compounds could come either from byproducts from side reactions of the radical ions or from excimer emission.

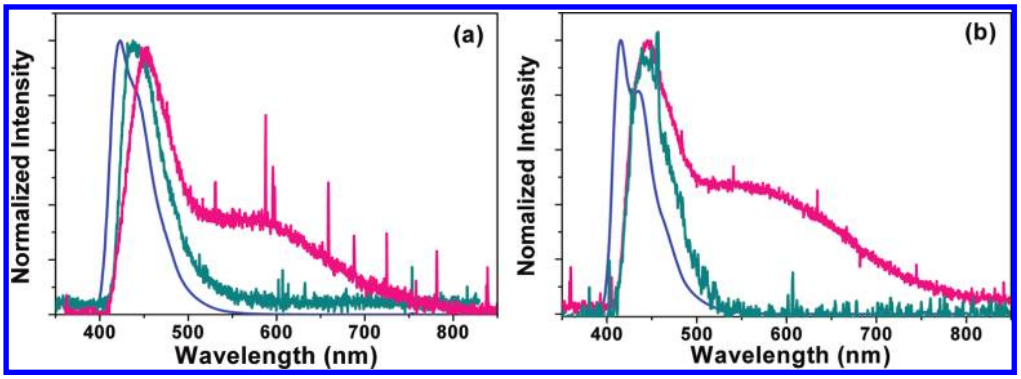

Figure 8. PL spectrum (blue line, 1 μM), ECL spectrum resulting from pulsing the electrode between −1.7 and 1.6 V vs Ag wire in BZN/0.1 M $TBAPF_6$ (pink line, 0.5 mM), and ECL spectrum generated with the coreactant BZN/0.1 M $TBAPF_6$/50 mM peroxydisulfate (green line) for (a) **4A** and (b) **4C**. ECL spectra were integrated 5 min using a 0.75 mm slit width.

Because the electrochemical result from reduction in BZN was irreversible and occurred near the solvent background, side reactions might have occurred. After the ECL experiment, the CV results showed similar waves, and the second ECL spectrum displayed a diminished intensity (Supporting Information Figure S9). However, when the electrode was polished, emission of ECL and electrochemistry were restored and showed two bands again with repeated pulsing. To confirm the secondary band from the byproducts, the PL spectrum of a solution was taken after extensive ECL cycling for 10 min. The PL spectra were similar before and after ECL measurement and did not show these longer wavelengths, so side reactions do not produce bulk amounts of products that emit at longer wavelengths. The other possibility is that the secondary broad band is due to the formation of an excimer. Compounds **4A** and **4C** are not good candidates to produce excimers because of their likely large steric hindrance with π-stacking between two molecules like DPA. However, as with spiro-FPA electrochemistry,[25] these compounds generate di- or tri-ions during oxidation and reduction, and these electrostatic attractions might overcome the steric hindrance to excimer formation. The formation of an excimer is more favorable in ECL than in PL because ECL is caused by the close proximity of the radical ions in a contact radical ion pair.[8,9]

The enthalpy of annihilation was estimated from the reversible standard potentials of the redox couples with the equation, $-\Delta H_{ann} = -\Delta G - T\Delta S = (E^{\circ}_{A^+/A} - E^{\circ}_{A/A^-}) - 0.1$ eV.[4] If the ECL reaction followed the S-route, the enthalpy of annihilation should be larger than the energy required to produce the excited singlet state from the ground state, E_s. Therefore, the singlet excited state can be directly populated by radical ion annihilation. The enthalpy of annihilation for two compounds calculated from the electrochemical data (shown in Table 1) is larger than the singlet energy from the emission spectra, so ECL via the S-route is a good possibility.

To estimate the stability of the ECL and the radical ion species, potential pulsing ECL transients were collected. When the potential was stepped from the reduction wave to the oxidation wave potentials, the same currents resulted, and the ECL intensity diminished on repeated pulsing (Supporting Information Figure S10). After the initial reduction, strong ECL emission appeared on the subsequent oxidation. After oxidation, very weak ECL emission appeared on the next reduction. This trend continued, with light-on cathodic pulses weaker than anodic ones, both gradually decreasing with continued pulse. For ECL systems where both radical ions are stable, pulses in both cathodic and anodic directions are essentially equal and are stable with time.[26] However, when the radical cation is unstable and decomposes during the anodic pulse, the emission is diminished on subsequent cathodic pulses, as found here. The relative ECL quantum yields of these compounds were determined by comparing the number of photons emitted per electron or annihilation event with that for the standard ECL emitter, DPA. The quantum yield of DPA in MeCN is ~8%.[17] This yielded ECL efficiencies of 0.0044 for **4A** and 0.0045 for **4C**.

Coreactant. When a radical is not sufficiently stable for ECL reaction or when a solvent has a narrow potential window for an ECL experiment to form the radical anions and cations, a coreactant is useful. A coreactant is a compound that can produce a strong oxidizing or reducing agent by a reaction that follows the electrochemical electron-transfer reaction. The coreactant must be energetic enough to oxidize or reduce radical ions of luminophores to produce their excited states. Tri-*n*-propylamine (TPrA),[27] oxalate ion ($C_2O_4^{2-}$),[28] and peroxydisulfate ($S_2O_8^{2-}$)[29] were used as coreactants. No ECL was seen with TPrA and $C_2O_4^{2-}$ because the products of these coreactants do not have sufficient reducing energy to react with the oxidized species to form the excited state (Supporting Information Figure S11).

Figure 8 shows the ECL spectra (green lines) of **4A** and **4C** in BZN with 50 mM coreactant, $S_2O_8^{2-}$, at a Pt electrode with 0.1 s pulse width from 0 to −2 V vs Ag QRE and 5 min integration time. Unlike the ECL spectra (pink lines) from ion annihilation, these ECL spectra displayed only one emission, which corresponds to their PL spectra (blue lines). This suggests that the products of the radical cations are contributors for excimer emission, although it is possible that long-wavelength emission is formed more efficiently in ECL than in PL by the radical ion annihilation. Peroxydisulfate generates a strong oxidant ($SO_4^{\bullet -}$) on reduction followed by bond cleavage. The E° value for the reduction of $SO_4^{\bullet -}$ has been reported to be ≥3.15 V vs SCE.[30] Thus, the intermediate, $SO_4^{\bullet -}$, has sufficient energy to generate the lowest excited state of these two compounds via eq 9. Moreover, the reduction of **4A** and **4C** produces radical anions (eq 9) at about −2.2 V vs SCE, which is more negative than required for the reduction of $S_2O_8^{2-}$, so that peroxydisulfate reduction can also occur via eq 10. The suggested mechanism is shown in Scheme 3.

Microscopic and Spectroscopic Measurements of 4A NPs. We fabricated **4A** NPs dispersed in water or MeCN by a

reprecipitation method. Unlike many aromatic compounds, **4A**, although soluble in DCM and THF, is not soluble in MeCN, which is a preferred solvent in ECL studies because of its wide electrochemical window to observe electrochemically generated radical cations and anions. A small amount of **4A** in a good solvent (THF) was injected rapidly and stirred vigorously into a poor solvent (either water or MeCN) to produce **4A** NPs. The size of NPs was controlled by the preparation conditions, i.e., the concentration of **4A** in THF, poor solvent temperature, stirring rate, and the method and speed of injection into the poor solvent. Figure 9 shows a TEM image of **4A** NPs dispersed in both water and MeCN. Because of the different miscibility of THF with water and MeCN, the sizes of **4A** NPs obtained were different. **4A** NPs prepared in water were significantly larger, ~40 nm, and had a less spherical shape than those in MeCN (Figure 9a,c). They were stable for only a few days. On the other hand, **4A** NPs dispersed in MeCN (15 ± 6 nm) produced spherical, small, and well-dispersed NPs (Figure 9b,d). Those NPs were stable for one week under ambient conditions without any surfactants.

Scheme 3

$$4A + e^- \rightarrow 4A^{\bullet -} \quad (9)$$

$$4A^{\bullet -} + S_2O_8^{2-} \rightarrow 4A + SO_4^{2-} + SO_4^{\bullet -} \quad (10)$$

$$4A^{\bullet -} + SO_4^{\bullet -} \rightarrow 4A^* + SO_4^{2-} \quad (11)$$

$$4A + SO_4^{\bullet -} \rightarrow 4A^{\bullet +} + SO_4^{2-} \quad (12)$$

$$4A^{\bullet +} + 4A^{\bullet -} \rightarrow {}^4A^* + 4A \quad (13)$$

$${}^4A^* \rightarrow 4A + h\nu \quad (14)$$

4A NPs were characterized on the basis of their optical properties by absorption and emission spectroscopy. Figure 10 shows the absorption and emission spectra of **4A** NPs dispersed in both water and MeCN as compared to that of **4A** molecule in THF. The absorption spectra of the **4A** NPs showed three strong vibronic peaks between 300 and 400 nm. The ratio of the three peaks, which can be taken as evidence of J- or H-aggregate formation, did not change. The absorption spectrum of the NPs dispersed in MeCN showed a tail in the long-wavelength region along with broadening of the peak widths. The fluorescence of NPs, taken with excitation at the absorption maximum of 400 nm, did not display a mirror image with respect to the absorption spectra. **4A** NPs dispersed in MeCN showed a single peak at 414 nm, which is blue-shifted by 10 nm as compared to that of the **4A** molecule in THF. However, **4A** NPs dispersed in water showed two peaks, at 414 and 434 nm. The difference in the absorption and emission spectra of the NPs compared with the molecules dissolved in an organic solvent showed little effect on particle size and no enhancement of fluorescence intensity or efficiency.

ECL of Organic NPs. The CV (Figure 11a) of the **4A** NPs dispersed in aqueous 0.1 M $NaClO_4$ displayed no distinctive peaks, and no ECL emission was observed because of the limited potential window in water, low concentration of NPs, and small

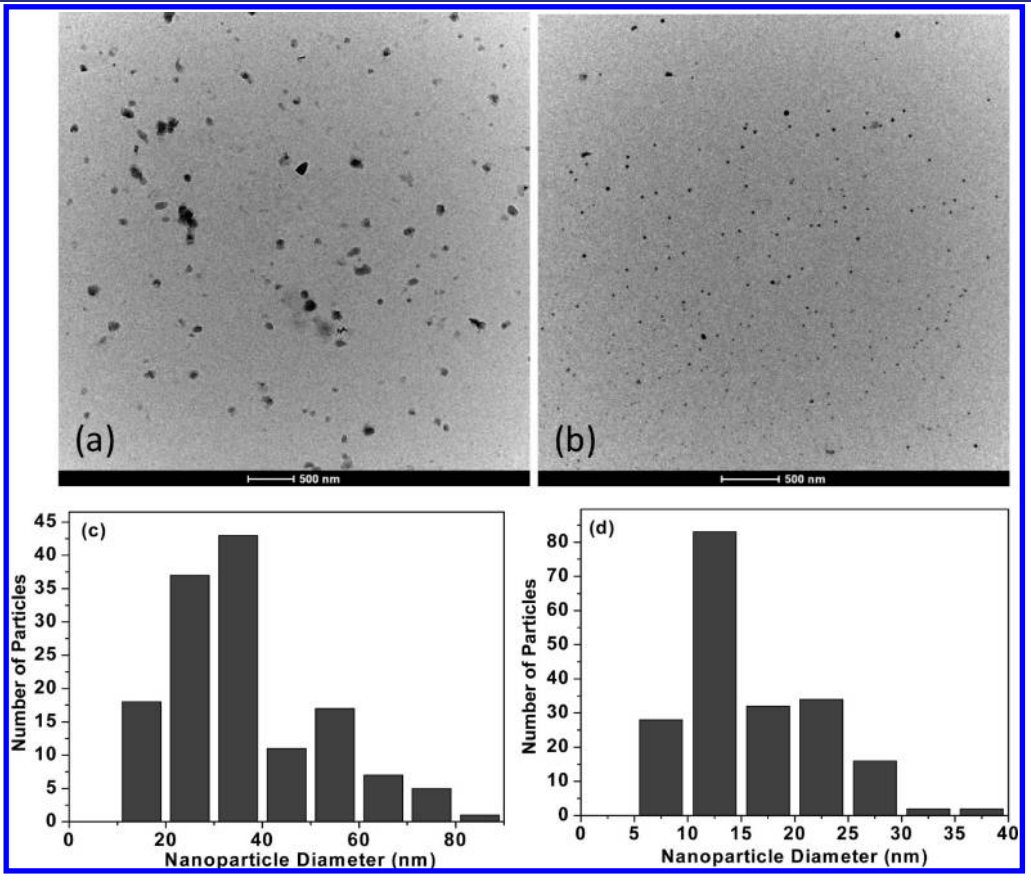

Figure 9. TEM images of (a) organic NPs of **4A** dispersed in water and (b) organic NPs of **4A** dispersed in MeCN. Histograms of size distribution of **4A** NPs: (c) average size of **4A** NPs dispersed in water is 40 ± 15 nm, and (d) average size of **4A** NPs dispersed in water is 15 ± 6 nm.

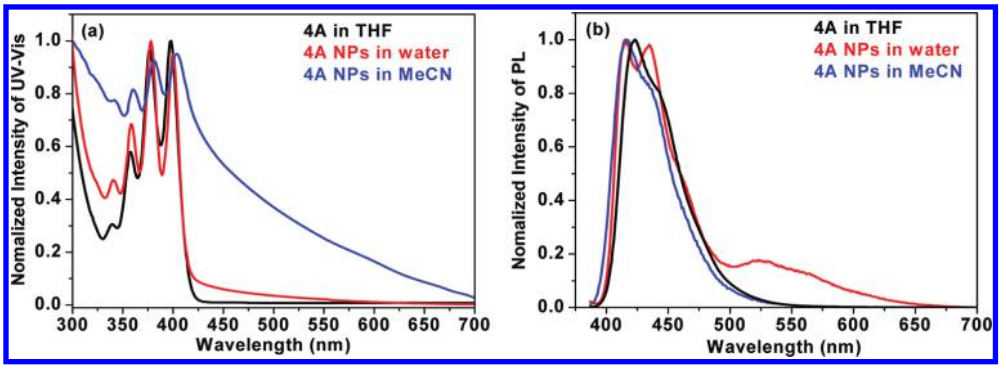

Figure 10. (a) Absorbance and (b) fluorescence spectra of **4A** and its NPs in various solvents. Emission spectra were excited at the absorption maxima.

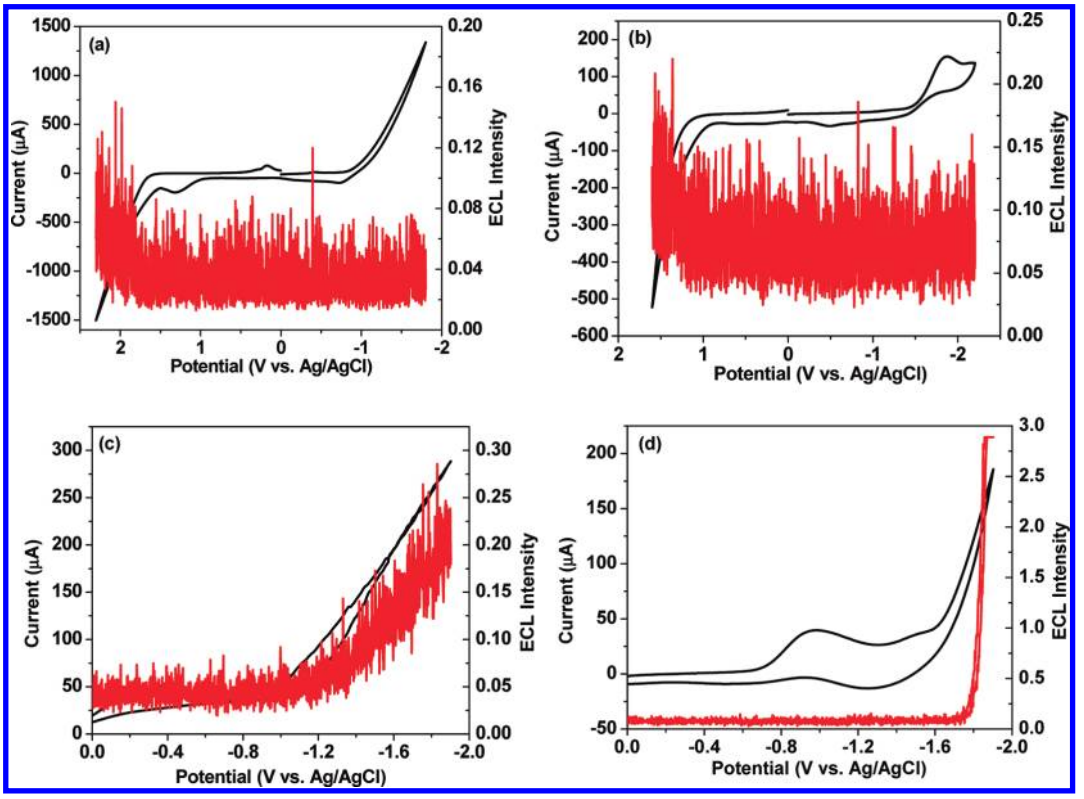

Figure 11. Cyclic voltammograms (black line) and ECL intensity (red line) of (a) **4A** NPs in room-temperature water with 0.1 M $NaClO_4$ at scan rate of 500 mV/s; (b) **4A** NPs in room-temperature water with 0.1 M $NaClO_4/S_2O_8^{2-}$ at scan rate of 50 mV/s; (c) **4A** NPs in MeCN with 0.1 M $TBAPF_6$ at scan rate of 500 mV/s; and (d) **4A** NPs in MeCN with 0.1 M $TBAPF_6/S_2O_8^{2-}$ at scan rate of 100 mV/s.

diffusion coefficients (due to their large radii). However, the CV (Figure 11b) of the **4A** NPs dispersed in MeCN was different, having a distinctive peak at around −1.8 V, which is similar to the potential region where reduction of the **4A** molecule occurs in THF. Weak but noticeable ECL emission from the annihilation reaction was produced when the potential was scanned toward first negative and then positive potentials.

We can obtain information about the redox behavior and the ECL emission of the NPs with a coreactant in both water and MeCN. For **4A** NPs dispersed in water, a much stronger ECL signal was observed (Figure 11c) when the potential was scanned from 0 to −1.8 V in 0.1 M $NaClO_4$ containing 0.1 M $K_2S_2O_8$ (a coreactant which forms a strong oxidizing agent, $SO_4^{\bullet-}$) ($E_{red} \geq 3.15$ V vs SCE)[30] on reduction. Moreover, strong ECL emission was produced by pulsing between 0 and −1.8 V. The intensity was stable with time but not strong enough to obtain an ECL spectrum (Figure 12a,b). A strong ECL signal was produced with **4A** NPs dispersed in MeCN when the potential was scanned from 0 to −1.8 V in 0.1 M MeCN containing 0.1 M $S_2O_8^-$ as coreactant (Figure 11d). As shown in Figure 12c,d, strong ECL emission was produced when the electrode potential was stepped from 0 to −1.7 V to reduce both NPs and $S_2O_8^-$. The increase of the ECL signal on cycling perhaps indicates adsorption with formation of an emitting film, although there is no evidence of electrode fouling. The ECL signal was strong enough to obtain an ECL spectrum (Figure 13, red line). The ECL spectrum of NPs dispersed in MeCN showed a blue emission peak at a wavelength of ~430 nm, which is close to the ECL peak of **4A** molecules dissolved

dx.doi.org/10.1021/ja203731n |J. Am. Chem. Soc. 2011, 133, 14675–14685

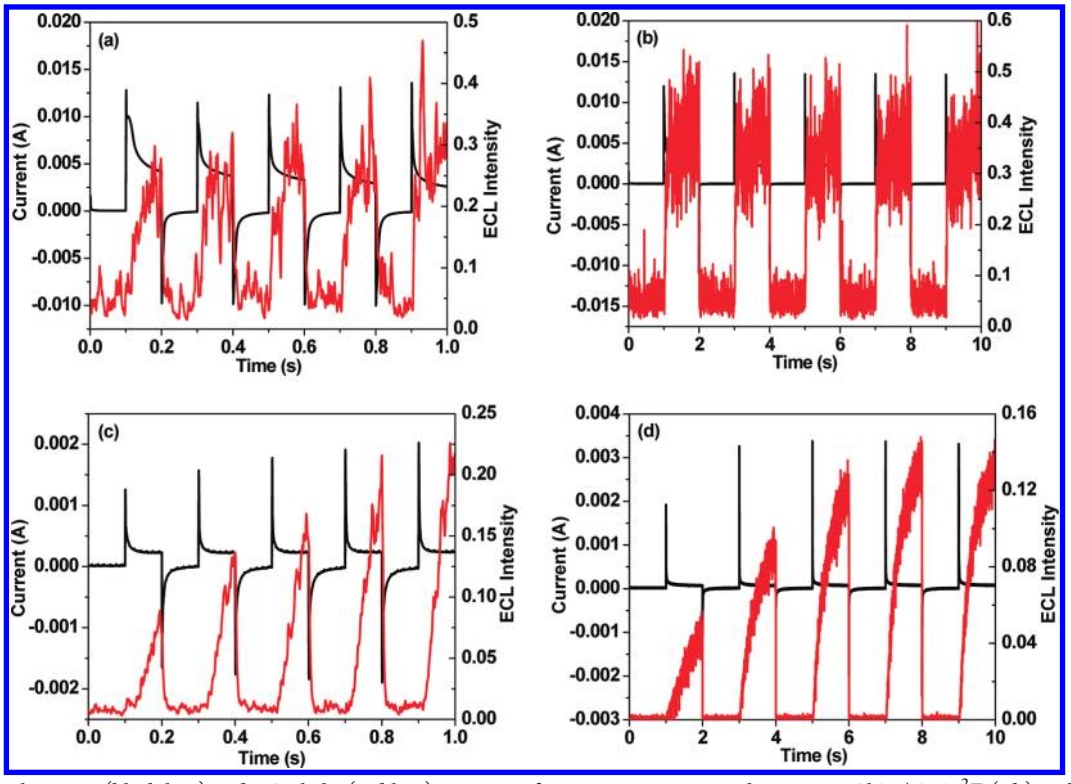

Figure 12. Initial current (black line) and ECL light (red line) transients for **4A** NPs in water with 0.1 M $NaClO_4$/ $S_2O_8^{2-}$ (a,b) and for **4A** NPs in MeCN with 0.1 M $TBAPF_6$/$S_2O_8^{2-}$ (c,d); sampling time, 1 ms. (a) Pulsing pattern, 0 to −1.8 V; pulse width, 0.1 s. (b) Pulsing pattern, 0 to −1.8 V; pulse width, 1 s. (c) Pulsing pattern, 0 to −1.7 V; pulse width, 0.1 s. (d) Pulsing pattern, 0 to −1.7 V; pulse width, 1 s.

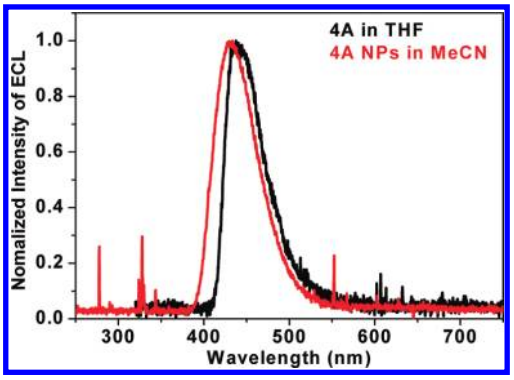

Figure 13. ECL spectra of **4A** molecules in THF with 0.1 M $TBAPF_6$/ $S_2O_8^{2-}$ (black line) and **4A** NPs in MeCN with 0.1 M $TBAPF_6$/- $S_2O_8^{2-}$ (red line).

in THF (Figure 13, black line). No longer-wavelength eximeric band was seen in the ECL spectrum of the NPs, perhaps because of the large surface area/volume ratio, as discussed for solid films.

CONCLUSION

Compounds **4A** and **4C**, consisting of two or three 9-naphthylanthracene groups, are good candidates for blue-light emitters. The 9-naphthylanthracene groups showed electrochemical processes at similar potentials with almost no communication among these groups because of the rigid and orthogonal center. Thus, **4A** and **4C** showed single and reversible oxidation and reduction waves in their CVs. For both compounds, ECL by ion annihilation produced two bands, assigned to monomer and excimer emission, which was not seen in the PL spectra of the solution state. However, ECL by reduction in the presence of $S_2O_8^{2-}$ as coreactant produced only monomer emission with similar PL wavelengths (in the solution state), suggesting the formation of excimer exclusively by radical ion annihilation. PL spectra of the film or powder state showed both monomer and excimer emission. Measurement of representative time traces of PL intensity, lifetimes, and picosecond TCSPC revealed the dynamics of the excimer emission. The results from **4A** showed stronger thickness-dependent effects of the longer wavelength intensity and broader and longer fluorescence lifetime distribution caused by maintaining optimized π-stacking compared to **4C**, which has distortion of π-stacking due to the propeller twist topology structure. We successfully prepared well-dispersed and spherical **4A** NPs in both water and MeCN by a simple reprecipitation method. The transient ECL generated from annihilation was weak but stable. A much stronger ECL signal from the NPs was produced with peroxydisulfate. Moreover, the intensity of **4A** NPs in MeCN with peroxydisulfate was stable with time and strong enough to obtain an ECL spectrum.

ASSOCIATED CONTENT

Supporting Information. Additional CV data. This material is available free of charge via the Internet at http://pubs.acs.org.

AUTHOR INFORMATION

Corresponding Author
ajbard@mail.utexas.edu; wanglei@mail.hust.edu.cn

■ ACKNOWLEDGMENT

We acknowledge support from Roche Diagnostics, Inc., the Robert A. Welch Foundation (F-0021), and the Doctoral Fund of the Ministry of Education of China (20100142120049). The authors thank Dr. Z. L. Huang for the TCSPC test.

■ REFERENCES

(1) Pope, M.; Kallmann, H. P.; Magnante, P. *J. Chem. Phys.* **1963**, *38*, 2042.

(2) (a) Lee, M. T.; Chen, H. H.; Liao, C. H.; Tsai, C. H.; Chen, C. H. *Appl. Phys. Lett.* **2004**, *85*, 3301. (b) Shi, J.; Tang, C. W. *Appl. Phys. Lett.* **2002**, *80*, 3201. (c) Ho, M. H.; Wu, Y. S.; Wen, S. W.; Lee, M. T.; Chen, T. M.; Chen, C. H.; Kwok, K. C.; So, S. K.; Yeung, K. T.; Cheng, Y. K.; Hao, Z. Q. *Appl. Phys. Lett.* **2006**, *89*, 252903. (d) Kim, M. S.; Choi, B. K.; Lee, T. W.; Shin, D. W.; Kang, S. K.; Kim, J. M.; Tamura, S.; Noh, T. Y. *Appl. Phys. Lett.* **2007**, *91*, 251111. (e) Gao, Z. Q.; Mi, B. X.; Chen, C. H.; Cheah, K. W.; Cheng, Y. K.; Wen, W. S. *Appl. Phys. Lett.* **2007**, *90*, 123506.

(3) Wang., L.; Wong, W.-Y.; Lin, M.-F.; Wong, W.-K.; Cheah, K.-W.; Tam, H.-L.; Chen, C. H. *J. Mater. Chem.* **2008**, *18*, 1.

(4) (a) Faulkner, L. R.; Bard, A. J. In *Electroanalytical Chemistry*; Bard, A. J., Ed.; Dekker: New York, 1977; Vol. 10, pp 1−95. (b) Faulkner, L. R.; Glass, R. S. In *Chemical and Biological Generation of Excited States*; Waldemar, A., Giuseppe, C., Eds.; Academic Press: New York, 1982; Chapter 6. (c) Richter, M. M. *Chem. Rev.* **2004**, *104*, 3003. (d) Knight, A. W.; Greenway, G. M. *Analyst* **1994**, *119*, 879.(e) Bard, A. J.; Debad, J. D.; Leland, J. K.; Sigal, G. B.; Wilbur, J. L.; Wohlstadter, J. N. In *Encyclopedia of Analytical Chemistry: Applications, Theory and Instrumentation*; Meyers, R. A., Ed.; John Wiley & Sons: New York, 2000; Vol. 11, p 9842. (f) Bard, A. J. *Electrogenerated Chemiluminescence*; Dekker: New York, 1998.

(5) (a) Birks, J. B. *Acta Phys. Pol.* **1968**, *34*, 603. (b) Birks, J. B. *Rep. Prog. Phys.* **1975**, *38*, 903.

(6) Birks, J. B.; Lumb, M. D.; Munro, I. H. *Proc. R. Soc. London* **1964**, *A280*, 289.

(7) (a) Winnik, F. M. *Chem. Rev.* **1993**, *93*, 587. (b) Kim, S. K.; Lee, S. H.; Lee, J. Y.; Lee, J. Y.; Bartsch, R. A.; Kim, J. S. *J. Am. Chem. Soc.* **2004**, *126*, 16499. (c) Lee, S. H.; Kim, S. H.; Kim, S. K.; Jung, J. H.; Kim, J. S. *J. Org .Chem.* **2005**, *70*, 9288. (d) Lee, J. Y.; Kim, S. K.; Jung, J. H.; Kim, J. S. *J. Org. Chem.* **2005**, *70*, 1463.

(8) Werner, T. C.; Chang, J.; Hercules, D. M. *J. Am. Chem. Soc.* **1970**, *92*, 763.

(9) Suminaga, T.; Hayakawa, S. *Bull. Chem. Soc. Jpn.* **1980**, *53*, 315.

(10) (a) Turro, N. J.; Hammond, W. B. *J. Am. Chem. Soc.* **1965**, *87*, 3259. (b) Werner, T. C.; Chang, J.; Hercules, D. M. *J. Am. Chem. Soc.* **1970**, *92*, 5560.

(11) Bard, A. J.; Park, S. M. In *The Exciplex*; Gordon, M., Ware, W. R., Eds.; Academic Press: New York, 1975; p 275.

(12) Chandross, E. A.; Longworth, J. W.; Visco, R. E. *J. Am. Chem. Soc.* **1965**, *87*, 3259.

(13) Park, S. M.; Bard, A. J. *J. Am. Chem. Soc.* **1975**, *97*, 2978.

(14) Faulkner, L. R.; Bard, A. J. *J. Am. Chem. Soc.* **1968**, *90*, 6284.

(15) Omer, K. M.; Bard, A. J. *J. Phys. Chem. C* **2009**, *112*, 11575.

(16) Sahami, S.; Weaver, M. *J. Electroanal. Chem.* **1981**, *122*, 155.

(17) Stevens, B.; Algar, B. *J. Phys. Chem.* **1968**, *72*, 2582.

(18) (a) Kasai, H.; Nalwa, H. S.; Oikawa, H.; Okada, S.; Matsuda, H.; Minami, N.; Kakuta, A.; Ono, K.; Mukoh, A.; Nakanishi, H. *Jpn. J. Appl. Phys. Part 2* **1992**, *31*, L1132. (b) Kasai, H.; Oikawa, H.; Okada, S.; Nakanishi, H. *Bull. Chem. Soc. Jpn.* **1998**, *71*, 2597. (c) Wu, C.; Peng, H.; Jiang, Y.; McNeill, J. *J. Phys. Chem. B* **2006**, *110*, 14148. (d) Kaneko, K.; Shimada, S.; Onodera, T.; Kimura, T.; Matsuda, H.; Okada, S.; Kasa, H.; Oikawa, H.; Kakudate, Y.; Nakanishi, H *Jpn. J. Appl. Phys.* **2007**, *46*, 6893. (e) Mori, J.; Miyashita, Y.; Oliveira, D.; Kasai, H.; Oikawa, H.; Nakanishi, H. *J. Cryst. Growth* **2009**, *311*, 553.

(19) Wong, K.-T.; Chien, Y.-Y.; Chen, R.-T.; Wang, C.-F.; Li, Y.-T.; Chiang, H.-H.; Hsieh, P.-Y.; Wu, C.-C.; Chou, C. H.; Su, Y. O.; Lee, G.-H.; Peng, S.-M. *J. Am. Chem. Soc.* **2002**, *124*, 11576.

(20) Bard, A. J.; Faulkner, L. R. *Electrochemical Methods: Fundamentals and Applications*, 2nd ed.; John Wiley & Sons: New York, 2001; pp 234−238.

(21) Denuault, G.; Mirkin, M. V.; Bard, A. J. *J. Electroanal. Chem.* **1991**, *308*, 27.

(22) Nakabayashi, T.; Wua, B.; Morikaw, T.; Iimori, T.; Rubin, M. B.; Speiser, S.; Ohta, N. *J. Photochem. Photobiol. A: Chem.* **2006**, *178*, 236.

(23) Yoo, H.; Yang, J.; Yousef, A.; Wasielewski, M. R.; Kim, D. *J. Am. Chem. Soc.* **2010**, *132*, 2929.

(24) Sartin, M. M.; Camerel, F.; Ziessel, R.; Bard, A. J. *J. Phys. Chem. C* **2008**, *112*, 10833.

(25) Sartin, M. M.; Shu, C.; Bard, A. J. *J. Am. Chem. Soc.* **2008**, *130*, 5354.

(26) Cruser, S; Bard, A. J. *J. Am. Chem. Soc.* **1969**, *91*, 267.

(27) (a) Smith, P. J.; Mann, C. K. *J. Org. Chem.* **1969**, *34*, 1821. (b) Noffsinger, J. B.; Danielson, N. D. *Anal. Chem.* **1987**, *59*, 865. (c) Leland, J. K.; Powell, M. J. *J. Electrochem. Soc.* **1990**, *137*, 3127. (d) Zu, Y.; Bard, A. J. *Anal. Chem.* **2000**, *72*, 3223. (e) Kanoufi, F.; Zu, Y.; Bard, A. J. *J. Phys. Chem. B* **2001**, *105*, 210. (f) Miao, W.; Choi, J.-P.; Bard, A. J. *J. Am. Chem. Soc.* **2002**, *124*, 14478.

(28) (a) Chang, M.-M.; Saji, T.; Bard, A. J. *J. Am. Chem. Soc.* **1977**, *99*, 5399. (b) Rubinstein, I.; Bard, A. J. *J. Am. Chem. Soc.* **1981**, *103*, 512. (c) Kanoufi, F.; Bard, A. J. *J. Phys. Chem. B* **1999**, *103*, 10469. (d) Miao, W.; Choi, J.-P.; Bard, A. J. *J. Am. Chem. Soc.* **2002**, *124*, 14478.

(29) (a) White, H. S.; Bard, A. J. *J. Am. Chem. Soc.* **1982**, *104*, 6891. (b) Bolletta, F.; Rossi, A.; Balzani, V. *Inorg. Chim. Acta* **1981**, *53*, L23. (c) White, H. S.; Bard, A. J. *J. Am. Chem. Soc.* **1981**, *104*, 6891. (d) Becker, W. G.; Seung, H. S.; Bard, A. J. *J. Electroanal. Chem.* **1984**, *167*, 127. (e) Fabrizio, E. F.; Prieto, I.; Bard, A. J. *J. Am. Chem. Soc.* **2000**, *122*, 4996.

(30) Memming, R. *J. Electrochem. Soc.* **1969**, *116*, 785.